Boundary Layers in Planes of Symmetry, Part II: Calculations for Laminar and Turbulent Flows

V. C. Patel* and J. H. Baek†
University of Iowa, Iowa City, Iowa

Comprehensive calculations of laminar and turbulent boundary layers in a plane of symmetry are made to explore the influence of mean-flow convergence and divergence. Comparisons are made with the experimental results presented in Part I, and with some previous data, to assess the gross effects of convergence and divergence on boundary-layer development and to evaluate the performance of a conventional turbulence model in the presence of the associated extra rates of strain.

I. Introduction

THE practical importance of plane-of-symmetry boundary layers and previous work on the subject were reviewed in Part I[1] of this paper. The experiments in turbulent flow reported therein revealed some of the peculiarities of such flows in spite of the limitations imposed by the rather thin boundary layer on the windward side. In order to obtain a more complete understanding of the effects of flow convergence and divergence on boundary-layer development in planes of symmetry, it is useful to supplement the somewhat limited experimental information with calculations. The purpose of this second part of the paper is to present the results of such a study. Here, we consider laminar as well as turbulent flow and make detailed comparisons with available experimental data for both.

II. Equations and Calculation Method

The different types of plane-of-symmetry flows are illustrated in Fig. 1, along with an appropriate coordinate system for boundary-layer calculations. $z=0$ is the plane of symmetry, and x and y are along and normal to the surface, respectively. (U,V,W) and (u,v,w) are the mean and fluctuating velocity components, respectively, in the (x,y,z) directions. Figure 1a shows a divergent flow ($W>0$). If the sign of W is reversed, we have a purely convergent flow. Figure 1b shows the case in which the boundary layer is subjected to a convergent external flow but with a region of divergent flow near the wall.

As noted in Ref. 1, the boundary layer in a plane of symmetry can be calculated independently of the flow on either side of it. Following Nash and Patel,[2] the boundary-layer equations, in the notation of Fig. 1 are

$$\frac{1}{h_1}\frac{\partial U}{\partial x}+\frac{\partial V}{\partial y}+\frac{1}{h_3}W_1+K_{31}U=0 \tag{1}$$

$$\frac{U}{h_1}\frac{\partial U}{\partial x}+V\frac{\partial U}{\partial y}+\frac{1}{h_1}\frac{\partial}{\partial x}\left(\frac{P}{\rho}\right)+\frac{\partial}{\partial y}(\overline{uv})-\nu\frac{\partial^2 U}{\partial y^2}=0 \tag{2}$$

$$\frac{U}{h_1}\frac{\partial W_1}{\partial x}+V\frac{\partial W_1}{\partial y}+W_1^2+K_{31}UW_1-\frac{U^2}{h_3}\frac{\partial K_{13}}{\partial z}+\frac{1}{h_3^2}\frac{\partial^2}{\partial z^2}\left(\frac{P}{\rho}\right)+\frac{\partial W_2}{\partial y}-\nu\frac{\partial^2 W_1}{\partial y^2}=0 \tag{3}$$

where

$$K_{31}=\frac{1}{h_1h_3}\frac{\partial h_3}{\partial x},\qquad K_{13}=\frac{1}{h_1h_3}\frac{\partial h_1}{\partial z}$$

$$W_1=\frac{1}{h_3}\frac{\partial W}{\partial z},\qquad W_2=\frac{1}{h_3}\frac{\partial}{\partial z}(\overline{vw}) \tag{4}$$

P is pressure, ρ density, and ν kinematic viscosity, and h_1 and h_3 are the metrics in the x and z directions, respectively. Equations (1) and (2) are the usual continuity and momentum equations, while Eq. (3) is obtained by differentiating the z momentum equation with respect to z and evaluating it on $z=0$. Thus, Eq. (3) gives the development of the rate of convergence or divergence, W_1.

The boundary conditions for the plane-of-symmetry flow are similar to those for two-dimensional flows. At the wall, $y=0$, the no-slip conditions are applied, i.e., $U=W_1=0$. For the flow outside the boundary layer, Eqs. (2) and (3) simplify to:

$$\frac{U_e}{h_1}\frac{\partial U_e}{\partial x}+\frac{1}{h_1}\frac{\partial}{\partial x}\left(\frac{P}{\rho}\right)=0 \tag{5}$$

$$\frac{U_e}{h_1}\frac{\partial W_{1e}}{\partial x}+W_{1e}^2+K_{31}U_eW_{1e}-\frac{U_e^2}{h_3}\frac{\partial K_{13}}{\partial z}+\frac{1}{h_3^2}\frac{\partial^2}{\partial z^2}\left(\frac{P}{k}\right)=0 \tag{6}$$

The pressure terms in Eqs. (2) and (3) can be eliminated by subtracting them from Eqs. (5) and (6). Then, at the edge of boundary layer, we have

$$U\to U_e,\qquad W_1\to W_{1e}\ \text{as}\ y\to\delta$$

where subscript e refers to the external flow. Thus, U_e and W_{1e} must be specified as functions of x. These have to be determined either from the potential-flow solution or from experiments.

For laminar flow, the Reynolds stresses $\overline{uv}$ and $\overline{vw}$ are zero, and Eqs. (1-3) are sufficient to determine U, V, and W_1 for a given pressure distribution. For turbulent flow, the

Received Dec. 30, 1985.

*Professor of Mechanical Engineering. Member AIAA.
†Research Assistant, Iowa Institute of Hydraulic Research; presently at Korea Advanced Institute of Science and Technology, Seoul, Korea.

isotropic, two-layer, eddy-viscosity model of Cebeci and Smith,[3] as modified in Refs 4 and 5, is adopted. This takes into account the effects of pressure gradients and low Reynolds numbers, as well as transition from laminar to turbulent flow through an empirical intermittency function. In general three-dimensional boundary layers, the Reynolds stresses are related to the local rates of strain by

$$-\overline{uv} = \nu_t \frac{\partial U}{\partial y}, \qquad -\overline{vw} = \nu_t \frac{\partial W}{\partial y} \tag{7}$$

where ν_t is the eddy viscosity. Then, the second equation yields

$$-W_2 \equiv \frac{1}{h_3}\frac{\partial}{\partial z}(-\overline{vw}) = \nu_t \frac{\partial}{\partial y}\left(\frac{1}{h_3}\frac{\partial W}{\partial z}\right) = \nu_t \frac{\partial W_1}{\partial y} \tag{8}$$

for the Reynolds-stress term in Eq. (3).

The calculation method chosen for this study is the Crank-Nicolson implicit method of Chang and Patel[6] since it is easily adopted for the solution of the plane-of-symmetry equations for laminar and turbulent flows and has been tested quite extensively for a variety of two-dimensional, axisymmetric, and three-dimensional flows. The numerical features of this method are described in detail in Ref. 6.

Calculations for two types of flow will be presented, namely, the flow ahead of a surface-mounted symmetrical body and the flow on a body of revolution at incidence. For the former, $h_1 = h_3 = 1$, $K_{13} = K_{31} = 0$, and $W_1 = \partial W/\partial z$. For the body of revolution whose local radius r is given as a function of axial distance X (see Fig. 1, Ref. 1), the z coordinate is replaced by the azimuthal angle θ, so that the metric coefficients h_1 and h_3 are $[1+(\mathrm{d}r/\mathrm{d}X)^2]^{1/2}$ and $r(X)$, respectively, and $W_1 = (1/r)(\partial W/\partial\theta)$. In most cases, calculations have also been performed assuming two-dimensional [i.e., Eqs. (1) and (2) with $W_1 = K_{31} = 0$] and axisymmetric flow [i.e., Eqs. (1) and (2) with $W_1 = 0$], with the same pressure distribution, to illustrate the relative effects of transverse curvature (K_{31}) and mean-flow convergence or divergence (W_1).

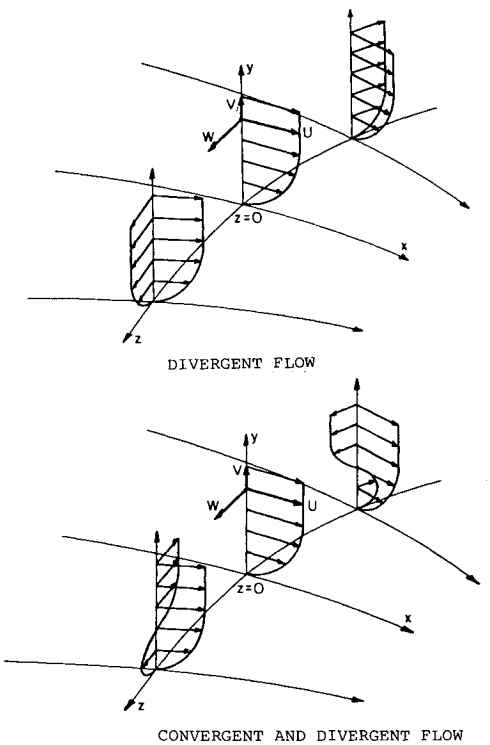

Fig. 1 Coordinate system for plane-of-symmetry boundary layers.

III. An Overview of the Calculations

The Crank-Nicolson method was first utilized to make a study of the laminar boundary layer on a prolate spheroid of axes ratio 4:1 over a range of incidences. These calculations were performed using the exact potential-flow solutions for U_e and W_{1e} with initial conditions specified just downstream of the potential-flow stagnation point. The results verified the major features of the earlier calculations of Wang[7,8] and Patel and Choi[9] but did not provide any new insights into either the numerical method or the physical phenomena involved. The DFVLR experiments of Meier, Kreplin, and others[10-13] on a 6:1 spheroid and present experiments described in Ref. 1, provided a fresh opportunity to evaluate the various numerical aspects of the calculation method by direct comparison with data and to study the problems associated with transition and turbulence modeling.

For clarity of presentation, it is convenient to classify plane-of-symmetry boundary layers in two categories: those subjected to mean-flow divergence (Fig. 1a) and those involving mean-flow convergence, or convergence and divergence simultaneously (Fig. 1b). In each case, we have selected examples of laminar as well as turbulent flow. The laminar-flow data obtained at the DFVLR are somewhat limited insofar as only the wall shear stresses were measured. Nevertheless, they can be used to evaluate the numerical aspects of the calculation method without the uncertainties of turbulence modeling. Secondly, the initial conditions are well defined since the solutions can be started at the stagnation point. For turbulent flow, the DFVLR data are again useful since they contain an initial region of laminar flow followed by natural transition and turbulent flow, and therefore a complete calculation can be performed by starting with the initial conditions at the stagnation point. On the other hand, the experiments of Ref. 1 provide greater detail in the turbulent boundary layer and can be used to assess the validity of the simple eddy-viscosity model.

IV. Boundary Layers with Flow Divergence

As noted earlier, the boundary layer in the windward plane of symmetry ($\theta = 0$ deg, see Fig. 1, Ref. 1) of a body at incidence is subjected to a continuous divergence of the external flow (i.e., $W_{1e} > 0$). This leads to a divergence of the mean flow within the boundary layer (i.e., $W_1 > 0$). A similar situation exists in the symmetry plane ahead of a symmetrical body standing on a flat surface.

Laminar Flow

The DFVLR experiments on the spheroid revealed that the flow in the windward plane remains laminar over a range of combinations of incidence α and Reynolds number Re up to the point of separation, which occurs just ahead of the sting at $X/L = 0.98$ used to mount the body in the wind tunnel. One such combination, for which tabulated data are available, is $\alpha = 30$ deg and $Re = 7.2 \times 10^6$. From the pressure distribution in Fig. 2a, we note that the measurements are in close agreement with potential-flow theory except over a short distance ahead of the sting at the tail.

The calculated distributions of wall shear-stress coefficient, $C_f = \tau_w/\frac{1}{2}\rho Q_0^2$, where Q_0 is the freestream velocity and τ_w the shear stress, and the momentum thickness, $\theta_{11} = \int_0^\delta U/U_e[1-(U/U_e)]\,\mathrm{d}y$, are shown in Fig. 2. It is seen that the calculated shear-stress distribution is in good agreement with the measurements. The small discrepancy may be due to the fact that the hot-film probes used to infer C_f were "calibrated" against a calculation method in axisymmetric flow. The calculations indicate separation ($C_f = 0$) very close to the tail, but the comparison with the data is not meaningful due to the support sting used in the experiments and the departure of the measured pressure distribution from that in potential flow. Calculations assuming two-dimensional and axisymmetric flow with the same pressure gradients are also presented in Fig. 2 to show the effects of trans-

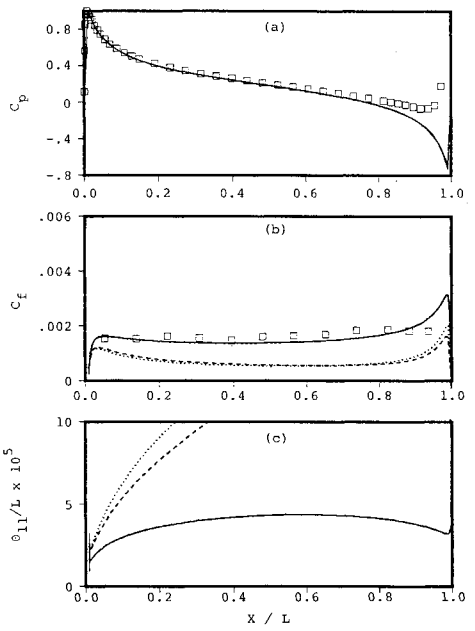

Fig. 2 Divergent laminar flow in the windward plane of the 6:1 spheroid, $\alpha = 30$ deg, and $Re = 7.2 \times 10^6$: □, experiment;——, plane of symmetry; - - -, axisymmetric; · · · , two-dimensional.

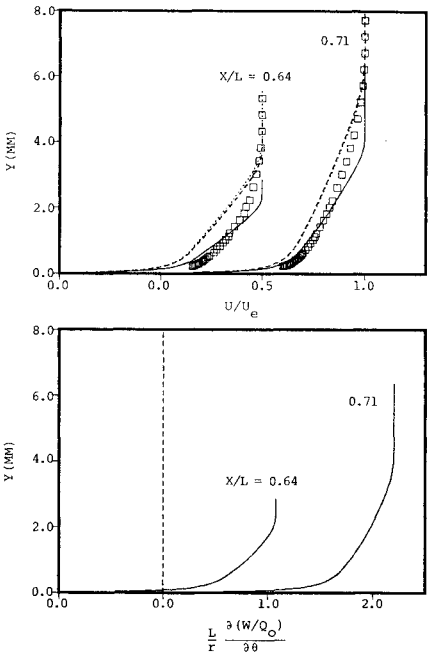

Fig. 4 Velocity profiles for the conditions of Fig. 3 (symbols as in Fig. 3).

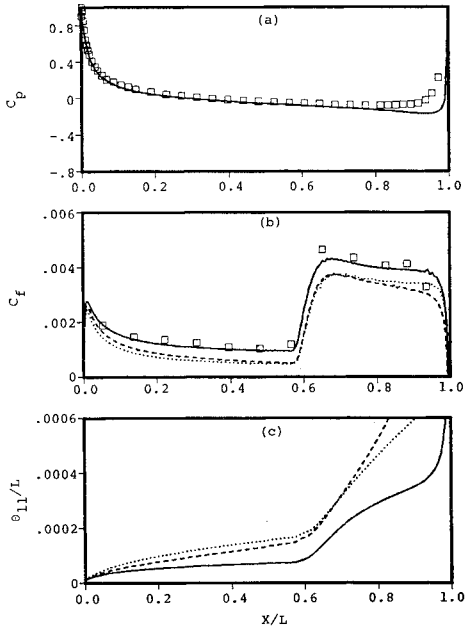

Fig. 3 Divergent laminar and turbulent flow in the windward plane of the 6:1 spheroid, $\alpha = 10$ deg and $Re = 7.2 \times 10^6$: □, experiment; ——, plane of symmetry; - - -, axisymmetric; · · ·, two-dimensional.

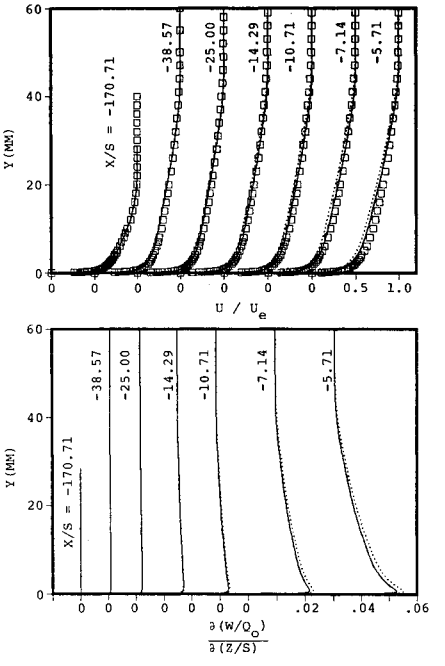

Fig. 5 Velocity profiles in the divergent turbulent boundary layer in the experiments of Krogstad: □, experiment; ——, measured U_e; · · ·, potential-flow U_e.

verse curvature and mean-flow divergence. It is seen that the former effect is not very significant but that the mean-flow divergence grossly inhibits the growth of the boundary layer.

Turbulent Flow

At an incidence of 10 deg and $Re = 7.2 \times 10^6$, the flow was observed to the laminar up to $X/L = 0.56$. The hot-film signals indicated that this was followed by a short region of natural transition and then turbulent flow. The experimental results are shown in Fig.3. In this case, the calculations were again started at the stagnation point, and transition was imposed at $X/L = 0.56$. The calculated wall shear-stress distribution is shown in Fig. 3b, and the corresponding momentum thickness is plotted in Fig. 3c. The calculations are in excellent agreement with the data not only in the laminar part but also in the turbulent part. The eddy-viscosity correlation of Cebeci et al. appears to mimic the changes in the transition zone quite effectively, at least with respect to the wall shear-stress variation.

In this case, the mean-velocity profiles were measured at two stations, namely, $X/L = 0.64$ and 0.71. Figure 4 shows a comparison with calculated profiles. The observed disagreement in the shape, as well as the rate of growth of the boundary layer is most probably due to the failure of the

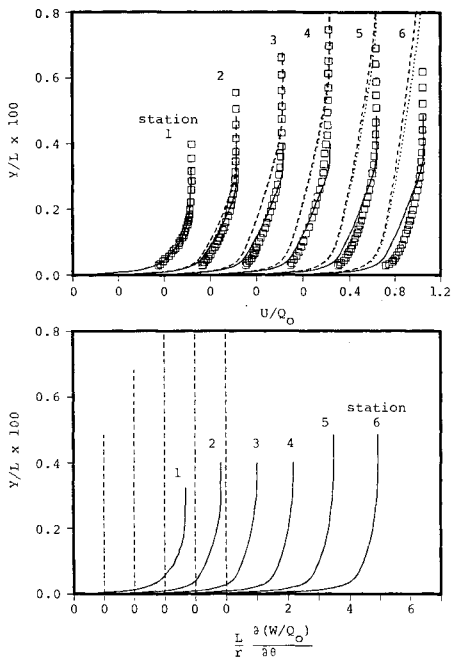

Fig. 6 Velocity profiles in the divergent (windward plane) turbulent boundary layer in the experiments of Ref. 1: □, experiment (yaw-probe data); ——, plane of symmetry; - - -, axisymmetric; · · ·, two-dimensional.

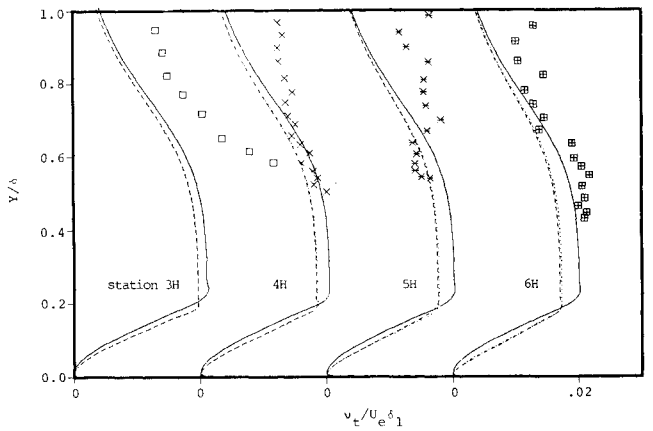

Fig. 7 Eddy-viscosity profiles in the divergent (windward plane) turbulent boundary layer in the experiments of Ref. 1: symbols denote experiment; ——, plane of symmetry; - - -, axisymmetric; · · ·, two-dimensional.

simple correlation used for the eddy viscosity, since the measurement stations are quite close to the transition point. Also shown in Fig. 4 are the corresponding calculated profiles of the rate of divergence, W_1. For later reference, we note that the shape of these profiles is quite similar to that of the longitudinal component of velocity, U/U_e.

Figures 3 and 4 include calculations for two-dimensional and axisymmetric flow. These comparisons reveal that transverse curvature is more important near the ends of the body where the curvature is large. However, the effect of mean-flow divergence is significant everywhere in the integral parameters as well as in the axial velocity profiles.

Of the many previous experiments involving turbulent boundary layers with mean-flow divergence, we have selected that of Krogstad,[14] who made measurements in the boundary layer on a flat plate ahead of a two-dimensional half-body generated by a simple two-dimensional source in a

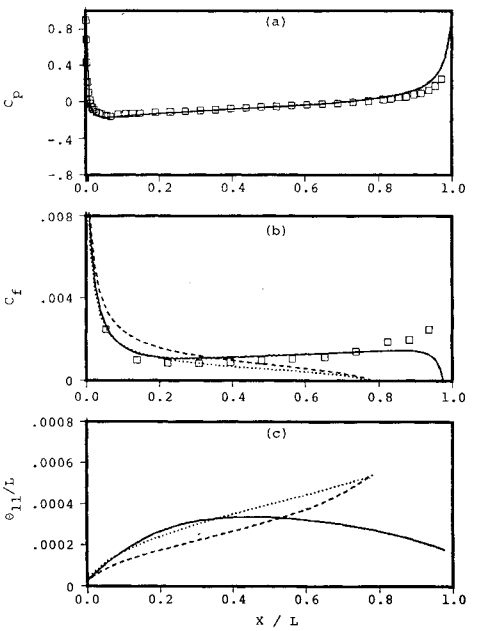

Fig. 8 Covergent and divergent laminar flow in the leeward plane of the 6:1 spheroid, $\alpha = 10$ deg and $Re = 1.6 \times 10^6$: □, experiment; ——, plane of symmetry; - - -, axisymmetric; · · ·, two-dimensional.

uniform stream. From a computational point of view, such flows are somewhat easier to deal with since the initial conditions are readily prescribed, i.e., the flow at a large distance ahead of the obstacle is two dimensional. In the present calculations, these were prescribed at $X/S = -170.7$, where S is the distance between the source and the stagnation point. The Reynolds number, based on the distance from the leading edge of the floor, at the initial station is 1.24×10^6. Most of the experimental results are concentrated in the range of the local Reynolds number $3\text{-}4 \times 10^6$. The calculations involve some uncertainties stemming from the prescription of the distribution of W_{1e} since the measured distribution of U_e was not exactly the same as that obtained from two-dimensional potential-flow theory and, therefore, W_{1e} will also not be the same as that in potential flow. Unfortunately, this information cannot be readily determined from the experiments. Consequently, the potential-flow distribution of W_{1e} was used, but two sets of calculations, corresponding to the theoretical and experimental distributions of U_e, were performed. The principal results of the calculations are shown in Fig. 5. The level of agreement seen is comparable to that obtained by Chang and Patel[6] for the case of East and Hoxey,[15] and by many other methods for similar flows (see, for example, the calculations performed by several different methods for a similar test case of the EUROVISC Workshop in Berlin[16]). The most significant aspect of such calculations is that they predict an earlier separation, the location of which is, of course, of great practical importance since it indicates the leading edge of the horseshoe vortex along the junction of the body with the plane. Although the predictions with the experimental values of U_e show some improvement, we note that, in general, the calculations underestimate the velocities throughout the boundary layer.

Although the two cases of turbulent flows considered above represent a test of the calculation method, they do not yield much direct information on the problem of turbulence modeling since turbulence measurements were not made. The experiments described in Ref. 1 were conducted to obtain such data. Unfortunately, as noted therein, the turbulence data on the windward side were restricted to the outer part of the rather thin boundary layer and consequently do not

provide a rigorous test. Nevertheless, it is of interest to present the corresponding calculations in order to demonstrate some general features of the solutions.

Since the experiments in Ref. 1 utilized a trip wire, the calculations could not be started at the stagnation point. Instead, the initial conditions were provided by the data at the most upstream station (station 1, $X/L=0.169$). Although this is a frequently adopted procedure in the evaluation of calculation methods for turbulent flows, it involves some uncertainty since the measured velocity profile provides only a part of the necessary information. Another quantity that must also be prescribed is the distribution of W_1 across the boundary layer, i.e., the initial rate of divergence. Since this could not be measured accurately, it was assumed that the initial profile of W_1 is similar to that of U, as indicated by the results shown in Fig. 4. Calculations were performed with these initial conditions and the streamwise distributions of U_e and W_{1e} obtained from the potential-flow solution. Comparisons between the measured and potential-flow pressure and edge-velocity distributions were presented and discussed in Ref. 1.

The comparisons between the boundary-layer calculations and experimental data are presented in Figs. 6 and 7. The results corresponding to two-dimensional and axisymmetric flow are also included. It is seen that the transverse-curvature effect is quite small but the mean-flow divergence has a large influence on the entire flow.

The mean-velocity and eddy-viscosity profiles calculated with the plane-of-symmetry equations are in reasonable agreement with the measurements, whereas the two-dimensional and axisymmetric-flow calculations show very significant differences. Closer examination indicates that even the plane-of-symmetry calculations tend to underestimate the velocity in the inner half of the boundary layer. This is presumably due to the failure of the turbulence model to account for the direct influence of flow divergence. Figure 6 also shows the calculated profiles of W_1, which is related to the extra rate of strain due to flow divergence. This increases monotonically from the wall to the outer edge of the boundary layer. However, the differences observed in the velocity profiles close to the wall do not appear to correlate simply with the extra rate of strain. Since detailed turbulence measurements could not be made in the inner half of the boundary layer, definitive conclusions cannot be drawn, but the eddy-viscosity comparisons of Fig. 7 indicate that the measured values are higher in the outer part of the boundary layer than those implied by the conventional model used here.

V. Boundary Layers Subjected to Flow Convergence

From a computational point of view, the plane-of-symmetry boundary layer subjected to convergence of mean flow from both sides, e.g., on the leeside of a body at incidence, poses the same problem as those encountered in the previous case. From a physical standpoint, however, the boundary-layer behavior is much more complex since pro-

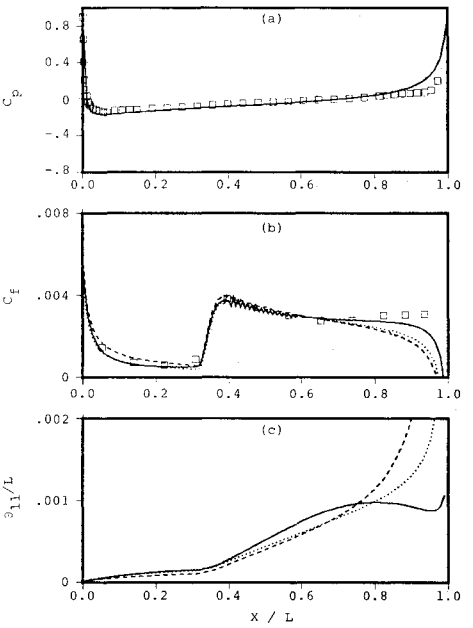

Fig. 10 Convergent and divergent laminar and turbulent flow in the leeward plane of the 6:1 spheroid, $\alpha=10$ deg and $Re=7.2\times10^6$: □, experiment; ——, plane of symmetry; - - -, axisymmetric; · · ·, two-dimensional.

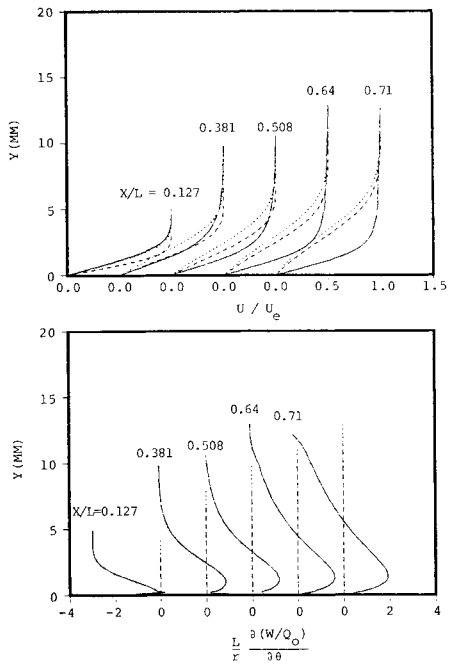

Fig. 9 Velocity profiles for the conditions of Fig. 8 (symbols as in Fig. 8).

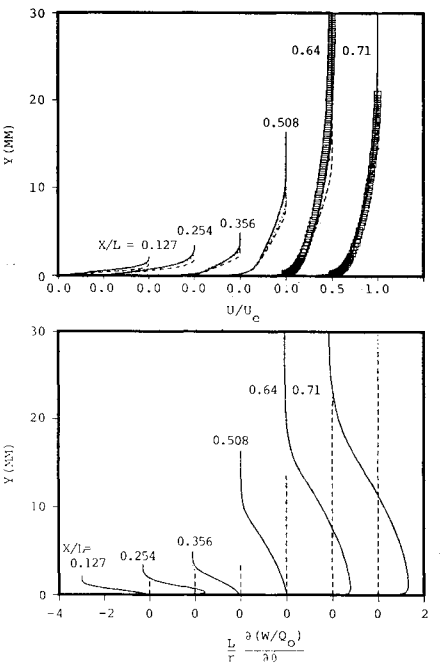

Fig. 11 Velocity profiles for the conditions of Fig. 10 (symbols as in Fig. 10).

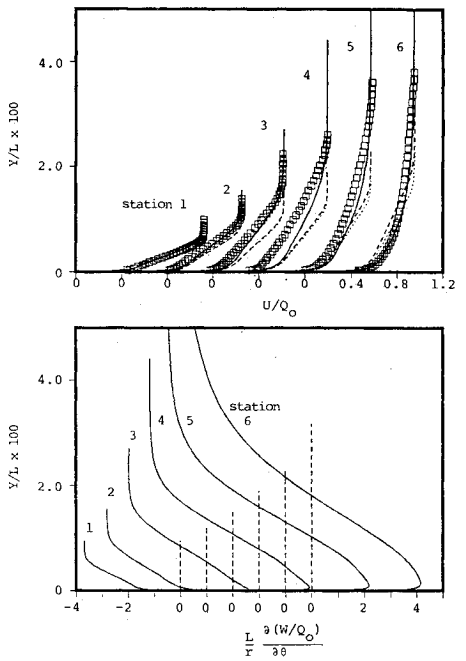

Fig. 12 Velocity profiles in the divergent (leeward plane) turbulent boundary layer in the experiments of Ref. 1: □, experiment (yaw-probe data); ——, plane of symmetry; - - -, axisymmetric; · · ·, two-dimensional.

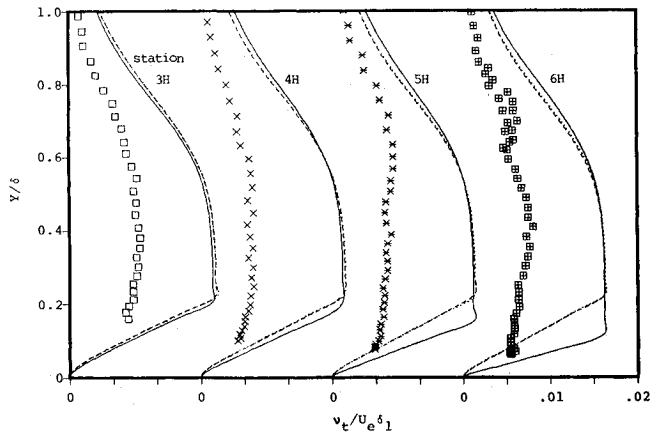

Fig. 13 Eddy-viscosity profiles in the divergent (leeward plane) turbulent boundary layer in the experiments of Ref. 1: symbols denote experiment; ——, plane of symmetry; - - -, axisymmetric; · · ·, two-dimensional.

longed convergence leads to a thickening of the boundary layer and the development of a region of flow divergence close to the surface. Thus, the boundary layer may be subjected to convergence and divergence simultaneously. Furthermore, the thickening of the boundary layer may be large enough to induce viscous-inviscid interaction.

As we remarked earlier, experiments in boundary layer with flow convergence are quite limited. On the DFVLR spheroid, wall shear-stress data are available for the cases $\alpha = 10$ deg, $Re = 1.6 \times 10^6$; $\alpha = 10$ deg, $Re = 7.2 \times 10^6$; and $\alpha = 30$ deg, $Re = 7.2 \times 10^6$. The flow on the leeward plane of symmetry is laminar in the first case but laminar and turbulent in the remaining two cases at the higher Reynolds number. However, we shall not consider the last case since it involves strong viscous-inviscid interaction. Because of the thicker boundary layer, the leeside data obtained in the experiments of Ref. 1 are more complete and can be used to test the calculation method in somewhat greater detail.

Laminar Flow

From the pressure distribution on the leeside of the spheroid at $\alpha = 10$ deg, $Re = 1.6 \times 10^6$ given in Fig. 8, it is evident that the agreement between theory and experiment is quite good since the boundary layer is thin and laminar. The results of the calculations are shown in Figs. 8 and 9. As before, the results of two-dimensional and axisymmetric flow calculations are also included. It is seen that the latter predict premature separation. On the other hand, the agreement of the plane-of-symmetry flow calculations with respect to the wall shear stress is seen to be as good as that observed earlier on the windward plane. Since velocity-profile measurements are not available for this case, direct comparisons cannot be made. However, the profiles of W_1 shown in Fig. 9 indicate a reversal in the sign of W_1 across the boundary layer as early as $X/L = 0.127$. The local flow divergence begins just ahead of this station. The magnitude of flow divergence and its extent, within the boundary layer, increase downstream, and associated with this is a reduced growth rate of the boundary-layer thickness.

Turbulent Flow

The results of the calculations for $\alpha = 10$ deg and $Re = 7.2 \times 10^6$ are presented in Figs. 10 and 11. The transition point was specified at the experimentally observed location, namely, $X/L = 0.31$. The predictions indicate excellent agreement with the data with regard to the wall shear-stress, as well as the velocity profiles, which were measured at two stations in the turbulent-flow region. The fluctuations in the calculations for the wall shear stress are due to the rapid changes in the numerical grid required to accommodate the rapidly increasing boundary-layer thickness (see Fig. 11). The success of the calculations through the transition zone is particularly noteworthy.

In Fig. 11, the profiles of longitudinal velocity clearly show the laminar, transitional, and turbulent-flow regions. The profiles of W_1 indicate several interesting features. Initially, at $X/L = 0.127$, the entire laminar boundary layer experiences convergent flow (i.e., $W_1 < 0$). A small region of flow divergence near the wall is observed at $X/L = 0.254$. This disappears as a result of transition, and at $X/L = 0.356$ and 0.508, the boundary layer is again subjected to pure convergence. However, a region of flow divergence reappears in the turbulent boundary layer at the downstream stations $X/L = 0.64$ and 0.71. Comparisons of the plane-of-symmetry flow calculations with two-dimensional and axisymmetric flow calculations are shown in Figs. 10 and 11. In the laminar region, the results show the same trends as in the case of the lower Reynolds number. In the turbulent-flow region, the measurements are in agreement with only the plane-of-symmetry flow calculations, which include the important effects of mean-flow convergence and divergence.

The calculations corresponding to the experiments of Ref. 1 presented the same difficulties as discussed earlier for the windward side. The initial conditions were again specified at $X/L = 0.169$, using the measured velocity profile and assuming that the initial distribution of W_1 across the boundary layer is similar to that of U/U_e. In this case, the subsequent solution was found to be highly sensitive to the initial distribution of W_1. The similarity assumption used here appeared to be the most reasonable one that could be made. The second uncertainty concerning the prescription of the axial variation of W_{1e} was also found to be somewhat greater on the leeside. The principal results of the calculations are shown in Figs. 12 and 13.

A comparison of Fig. 12 with Fig. 6 on the windward side shows that the disagreement between the measured and calculated velocity profiles is largest near the wall and in opposite directions. It is interesting to note that the agreement improves somewhat in the downstream direction, as is also observed in the spheroid experiments (Fig. 11). This improvement is perhaps due to the increasing region of flow

divergence ($W_1 > 0$) developing in the wall region which, according to Fig. 12, starts between stations 2 and 3. The overestimation of the velocity by the calculation method is consistent with the overestimation of the eddy viscosity shown in Fig. 13. The results of the two-dimensional and axisymmetric flow calculations confirm the importance of mean-flow convergence and divergence in the mean-flow equations. However, it is also clear that the net effect of flow convergence on the turbulence is to decrease the Reynolds stress and the eddy viscosity. The predictions with the complete plane-of-symmetry equations could therefore be improved by incorporating an extra rate-of-strain effect in the turbulence model. Although empirical correlations for extra strain effects due to factors such as curvature, rotation, and buoyancy have been suggested in the literature, the authors are not aware of the such corrections for the effect of lateral convergence or divergence.

VI. Conclusions

The comparisons between the calculations and experimental data for plane-of-symmetry boundary layers lead to the following observations.

1) In laminar flow, the calculations yield quite accurate predictions for both convergent and divergent flows, provided regions of strong viscous-inviscid interactions (which are observed on the leeside of bodies of revolution at large incidences) are excluded.

2) Extensive comparisons made between the plane-of-symmetry flow calculations and those using two-dimensional and axisymmetric-flow assumptions clearly indicate the gross effects of mean-flow convergence and divergence.

3) For turbulent flow, the experiments of Ref. 1 and the present calculations indicate a consistent and direct influence of the rate of convergence and divergence on the mean-velocity profiles and eddy viscosity. The influence of convergence is opposite to that of divergence, with convergence leading to a reduction in eddy viscosity. Thus, further improvements in the calculation method can be made by incorporating such an effect in the turbulence model. It would also be of interest to repeat these calculations using other turbulence models.

4) Since the flow in the plane of symmetry serves as a boundary condition for the complete three-dimensional boundary layer on a body, the preceding observations should be taken into account in the evaluation of calculation methods and turbulence models for the general three-dimensional case.

Acknowledgments

This research was supported by the U.S. Army Research Office and U.S. Air Force Office of Scientific Research under Grant AFOSR-80-0148B. The authors also acknowledge the assistance of Dr. A. W. Fiore of AFFDL and Dr. H. U. Meier of the DFVLR, project officers of the USAF-FRG Data Exchange Agreement, in making available tabulated data from the DFVLR experiments.

References

[1]Patel, V. C. and Baek, J. H., "Boundary Layers in Planes of Symmetry. Part I: Experiments in Turbulent Flow," *AIAA Journal*, Vol. 25, April 1987, pp. 550–559.

[2]Nash, J. F. and Patel, V. C., *Three Dimensional Turbulent Boundary Layers*, SBC Tech Books, Atlanta, GA, 1972.

[3]Cebeci, T. and Smith, A. M. O., "A Finite-Difference Solution of the Incompressible Turbulent Boundary-Layer Equations by an Eddy-Viscosity Concept," *Proceedures of the AFOSR-IFP-Stanford Conference: Computation of Turbulent Boundary Layers*, Vol. 1, edited by S. J. Kline, M. V. Morkovin, G. Sovran, and D. J. Cockrell, 1968.

[4]Cebeci, T. and Mosinskis, G. J., "Calculation of Incompressible Turbulent Boundary Layers at Low Reynolds Number," *AIAA Journal*, Vol. 9, Aug. 1971, pp. 1632–1634.

[5]Cebeci, T., "Calculation of Compressible Turbulent Boundary Layers with Heat and Mass Transfer," *AIAA Journal*, Vol. 9, June 1971, pp. 1091–1097.

[6]Chang, K. C. and Patel, V. C., "Calculation of Three-Dimensional Boundary Layers on Ship Forms," Iowa Institute of Hydraulic Research, Univ. of Iowa, IIHR Rept. 205, 1975.

[7]Wang, K. C., "Three-Dimensional Boundary Layer near the Plane of Symmetry of a Spheroid at Incidence," *Journal of Fluid Mechanics*, Vol. 43, Aug. 1970, pp. 187–209.

[8]Wang, K. C., "Laminar Boundary Layer near the Symmetry Plane of a Prolate Spheroid," *AIAA Journal*, Vol. 12, July 1974, pp. 949–958.

[9]Patel, V. C. and Choi, D. H., "Calculation of Three-Dimensional Laminar and Turbulent Boundary Layers on Bodies of Revolution at Incidence," *Turbulent Shear Flows II*, Springer-Verlag, New York, 1980, pp. 199–217.

[10]Meier, H. U. and Kreplin, H. P., "Experimental Investigation of Boundary Layer Transition and Separation on a Body of Revolution," *Zeitscrift für Flugwiss Weltraumforschung*, Vol. 4, No. 2, Aug. 1980, pp. 65–71.

[11]Kreplin, H. P., Vollmers, H., and Meier, H. U., "Experimental Determination of Wall Shear Stress Vectors on an Inclined Prolate Spheroid," *Proceedings of the 5th USAF-FRG Data Exchange Agreement Meeting*, Tech. Rept. AFFDL-TR-80-3088, 1980, pp. 315-332.

[12]Meier, H. U., Kreplin, H. P., and Vollmers, H., "Velocity Distributions in 3-D Boundary Layers and Vortex Flows on an Inclined Prolate Spheroid," *Proceedings of the 6th USAF-FRG Data Exchange Agreement Meeting*, DFVLR-AVA Rept. IB 22281 CP1, 1981, pp. 202–217.

[13]Kreplin, H. P., Vollmers, H., and Meier, H. U., "Measurements of the Wall Shear Stress on an Inclined Prolate Spheroid," *Zeitschrift für Flugwiss Weltraumforschung*, Vol. 6, No. 4, 1982, pp. 248–252.

[14]Krogstad, P. A., "Investigation of a Three-Dimensional Turbulent Boundary Layer Driven by Simple Two-Dimensional Potential Flow," Dr.-Ing. Thesis, Norwegian Institute of Technology, Trondheim, Norway, 1979.

[15]East, L. F. and Hoxey, R. P., "Low-Speed Three-Dimensional Turbulent Boundary Layer Data. Part 1," British Aeronautical Research Council, R & M 3653, 1969.

[16]van den Berg, B., Humphreys, D. A., Krause, E., and Lindhout, J. P. F., "Computation of Three-Dimensional Boundary Layers," *Proceedings of EUROVISC Workshop*, Berlin, FRG, April 1982, to be published.